Short communication

In situ FT-IR reveals ageing phenomena in the formation of a Cu/Zn/Zr methanol catalyst precursor

Lucas Warmuth [*] , Thomas A. Zevaco , Stephan Pitter

Institute of Catalysis Research and Technology (IKFT), Karlsruhe Institute of Technology (KIT), Hermann-von-Helmholtz-Platz 1, 76344 Eggenstein-Leopoldshafen, Germany

ABSTRACT

CO_2-rich feeds reduce the carbon footprint of methanol using ZrO_2-promoted Cu/ZnO catalysts. Suspension aging is crucial for efficient production of those, likewise for Cu/ZnO/Al_2O_3 systems. We identified and tracked markers by *in/ex situ* FTIR, required to deliver targeted zincian malachite. In addition, morphological changes revealed by electron microscopy could be correlated to the respective time-resolved spectra. Based on this, the optimization of the catalyst production process will be simplified.

1. Introduction

Reducing the carbon footprint of methanol, an important platform chemical with several further use and increasing demand (2015: $\approx$75 Mt; 2020: $\approx$110 Mt; 2025 estimate: $\approx$145 Mt), is a necessary target for mitigating climatic changes [1–6]. Employed industrial methanol Cu/ZnO/Al_2O_3 (CZA) catalysts are used for conversion of synthesis gas with less than 10 % CO_2 content and have been studied thoroughly [7–12]. CO_2-rich feeds can be provided by industrial CO_2 point sources and their conversion is reported to be promising with Cu/ZnO/ZrO_2 (CZZ) catalysts. These are described to overcome this change in feedstock resulting in additional water formation by higher water tolerance still showing good methanol productivity and acceptable stability [13–16].

Systematic optimization of the aging step requires a detailed knowledge of the evolution of the crystal phases during said process by diverse investigation techniques generally applied for Cu/Zn (CZ) systems [7,17–25]. According to the state of research for CZA catalysts, an optimal precatalyst mainly consists of a malachite phase [(Cu, Zn)$_2$(OH)$_2$CO$_3$] with maximum Zn incorporation [17,26], providing most efficient Cu–Zn interactions in the catalyst after calcination and activation, particularly indicated by high specific surface areas and active metallic (Cu) surface areas [27].

Recently, we described a CZZ catalyst preparation method (see Fig. 1) using an optimized sequence of continuous co-precipitation

followed by controlled batch-wise aging. This approach turned out to be highly favorable towards catalyst homogeneity, scalability of catalyst preparation and high activity in methanol synthesis [28,29]. Technically, initial nucleation takes place directly downstream in a micromixer under highly turbulent conditions on a millisecond time scale continuously delivering an amorphous precipitate at steady-state conditions, ready for subsequent aging [28]. In order to experimentally elucidate the thermodynamically controlled aging, its spatial and temporal separation from the kinetically determined initial precipitation is a significant advantage [29]. Thus, in contrast to the typically applied precipitation induced by dropwise addition of two stock solutions (e.g. metal nitrate salts and carbonate/bicarbonate, Fig. 1, top) into the same vessel where aging is actually beginning, our approach specifically comprises a very short mixing time and hence, a significantly reduced nucleation period P in relation to the total aging period (Fig. 1, bottom). Advantageously, this also results in minimized temporal overlap between precipitation and aging periods.

Güldenpfennig *et al.* characterized the so-called tipping point from *in situ* FTIR monitoring during the aging period, indicating the recrystallization of an amorphous phase (assumedly georgeite) to crystalline malachite-type phases, also supported by pH monitoring data [24]. The authors observed a sharp increase of two distinct absorptions at around 1020 and 1120 cm^{-1} both attributed to M—OH deformation vibrations. Similarly, a detailed study focussing on the substitution of Mg into the
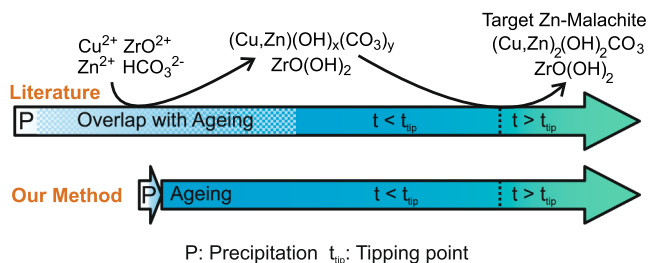

Fig. 1. Preparation sequence depicting co-precipitation and aging yielding precursors of CuO/ZnO/ZrO₂ (after calcination). In comparison to typical sequences comprising a longer precipitation period (batch-wise/batch-wise), this work investigates the aging step in a largely decoupled manner by realizing a very short period for initial nucleation (continuous/batch-wise). t_{tip}: Tipping point, P: initial nucleation/precipitation.

malachite crystal lattice and following its insertion over time, including *in situ* FTIR spectroscopy, was published by Behrendt and co-workers [30]. Nevertheless, a description of the relevant phases occurring throughout the suspension aging remains challenging.

2. Results and discussion

In situ IR spectroscopy should enable practical insight into complex aging phenomena and the related phase transformations that occur in the process, even if the materials may be amorphous. The main absorption bands recorded *in situ* during the ongoing precipitation and suspension aging steps belong to nitrate-, carbonate- and hydroxy-containing species of the metals involved (Cu, Zn, Zr). Due to similarities in the coordination geometries of nitrate and carbonate anions (D_{3h} point group), the expected vibrations of both ions in the relevant region are very similar. Fig. 2a shows the changes in relative absorbance detected by *in situ* FT-IR/ATR measurement during aging of CZZ precursor suspension. In order to support this IR monitoring, scanning electron microscopy was used in combination with energy-dispersive X-ray spectroscopy (SEM/EDXS) to assess possible connections between collected IR data and morphology of the materials (Fig. 3).

The broad and weak absorption around 1560 cm⁻¹, for $t > t_{tip}$ indicates the presence of mono- or bidentate CO_3^{2-}. Strong absorption bands at 1310 and 1340 cm⁻¹ (only visible beyond the tipping point / crystallization of malachite: $t > t_{tip}$) are attributed to either CO_3^{2-} (possibly monodentate; [31] symmetric stretching, ν_3) [32,33] or NO_3^- (symmetric stretching) [34,35]. The second strongest vibration at 1474 cm⁻¹, likewise only observable at $t > t_{tip}$, is also ascribed to CO_3^{2-} (asymmetric stretching, ν_3) [36], which indicates formation of the malachite phase. Some weaker overlapping vibrations in the 1000–1100 cm⁻¹ region (1104/1056/1007 cm⁻¹) indicate the presence of CO_3^{2-} (symmetric stretching, ν_1) [33], NO_3^- (symmetric stretching ν_1) [34], OH [37–39], CO_3^{2-} (both out-of-plane deformation vibrations) [32,33,37], HCO_3^-[40] or monodentate CO_3^{2-}[41,42] (—CO—H or —CO—M symmetric stretching) fragments, respectively. This assignment is in good agreement with recently published results on promoter-free Cu/ZnO precursor formation [30].[1]

In order to cross-check results from *in situ* IR spectroscopy and to exclude signals of dissolved species (e.g. NO_3^-), additional *ex situ*

measurements were performed on samples withdrawn after defined aging times, followed by washing and drying. Aside from the absorptions observable *via in situ* FTIR, additional bands at lower energy are detected, tentatively attributed to stretching vibrations from metal oxide/hydroxide moieties (ν(Cu/Zn-O) and ν(Cu/Zn—OH); Fig. 2b). Comparing the numerous single transmission spectra reveals that the expired period until $t > t_{tip}$ is reflected to be nearly the same as from *in situ* ATR measurements (49 min *ex situ* vs. 50 min *in situ*). The most significant changes between *ex-* and *in situ* spectra are the red-shift of some bands attributed to carbonate (ν_3) vibration and the disappearance of HCO_3^- [40] or monodentate CO_3^{2-} [41,42] (COH or CO—M stretch) at 1007 cm⁻¹ for *ex situ*. This points out that the precipitate is characterized by absorption bands that are obviously not detected with the same sensitivity *in situ* (using Attenuated Total Reflectance) and *ex situ* (using KBr pellets with transmission technique; SI: Table S1). *Ex situ* spectra (Fig. 2b; t = 9 min) indicate georgeite as the main initial component of the suspension [39,43], whereas SEM/EDXS reveals spherical particles with Zn inhomogenities (Fig. 3). These inhomogenities may be due to segregation of Zn-rich species occuring in small amounts (e.g. $Na_2Zn_3(CO_3)_4 \times 3\ H_2O$ [19] or hydrozincite $Zn_5(OH)_6(CO_3)_2$) and are topic of further research. Due to the inherent higher resolution of *ex situ* measurements recorded in transmission modus, the less intense absorptions of aurichalcite at 965 cm⁻¹ (ν(MO—H)) are also detected during this period (9–29 min). In addition, a characteristic carbonate bending mode (ν(CO₃) at 831 cm⁻¹ indicates the presence of aurichalcite [37,44]. Thus, aurichalcite formation also starts at an early stage ($\geq$9 min), whereas malachite is observable at this point, too. The formed aurichalcite is most likely crystalline and incorporates the Zn inhomogenities as shown by SEM/EDXS.

Throughout later aging, malachite arises (>29 min; 821/1051/1100 cm⁻¹) [37] and increases in intensity while georgeite and aurichalcite disappear and are not detectable anymore from 49 min onwards. This corresponds to the literature-known tipping point, also indicated by some typical pH drop (Fig. 2, right side). Interestingly, after 49 min of aging, the already crystallized malachite phase observable in FTIR temporarily disappears and reappears at 59 min. A likely explanation for this is that a recrystallization step involving the liquid phase is taking place, yielding mixed zincian malachite/rosasite out of the former aurichalcite/malachite mixture. The proposed recrystallization step is supported by SEM images, which display spherical particles around 49 min ageing time, which further transform into rod-shaped nanostructures at 59 min, a morphological pattern typical for CZ catalyst precursors [45]. Understanding the underlying mechanism ruling this recrystallization step will be the topic of further specific studies.

3. Conclusion

By combining *in situ* FTIR (using attenuated total reflectance) with *ex situ* methods (SEM/EDXS; FTIR transmission; using KBr pellet), we found out that monitoring specific, transient FTIR absorption bands deliver highly relevant information on the progress of the suspension aging within the synthesis of CZZ precursors. According to literature on CZ and CZA precursors, the presence of a copper-zinc hydroxycarbonate (malachite) phase plays a predominant role in the formation of materials with the right composition and morphology to deliver efficient methanol catalysts upon calcination.

Our data obtained from *ex situ* measurements confirm key features of the *in situ* measurements, especially regarding the changes at the tipping/crystallization point. Apart from the increased effort, whereas the accurate determination of the aging time for *ex situ* is strictly limited by the sampling frequency, our comparison also underlines that *in situ* FTIR obviously allows for precise and real-time recognition of the tipping point. The separation of the phenomena occurring shortly after the initial nucleation from those happening during aging is made possible by the application of the "continuous/batch" procedure with a micromixer upstream of the aging tank. Particular advantages of *in situ*
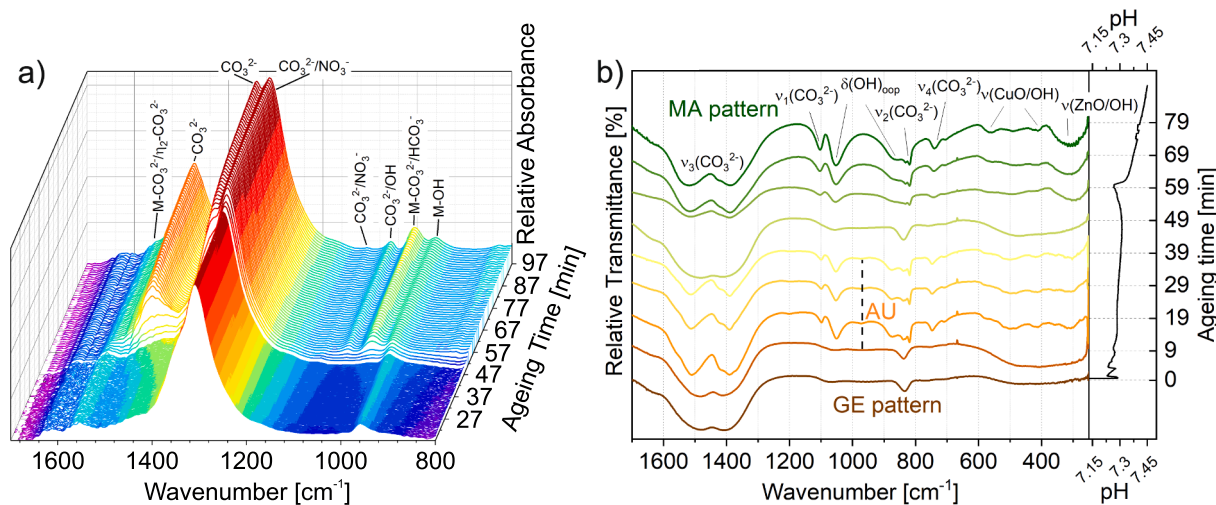
---

[1] However, assigning absorption bands in the region below 1000 cm⁻¹ is complex, owing to the fact that bands of similar energies from the hydroxy deformation mode could be also present. For instance, a weak absorbance remaining throughout the aging step at 959 cm⁻¹ can be either attributed to a metal-OH vibration in malachite $Cu_2(CO_3)(OH)_2$ [37] or azurite [43]. Absorptions lower than 780 cm⁻¹ are not analysed by the ATR device used in this work. The very weak absorbance around 825 cm⁻¹ (for $t > t_{tip}$ only) can be tentatively described as a combination of vibrations from NO_3^- (asymmetric stretching, ν_2) [34] and CO_3^{2-} (scissoring, ν_4) [33,37].

Fig. 2. (a) *In situ* FTIR Waterfall plots recorded during aging of CZZ precursor in the spectral region 1700–800 cm^{-1}. (b) *Ex situ* FTIR of samples withdrawn, washed and dried at defined times of suspension aging, beginning after initial nucleation (bottom) to the endpoint (top). For reference, the pH evolution is shown on the right side revealing the typical local pH minimum indicating the "tipping-point". The typical georgeite (GE) and malachite (MA) patterns are visible as well as one main vibration of aurichalcite (AU).
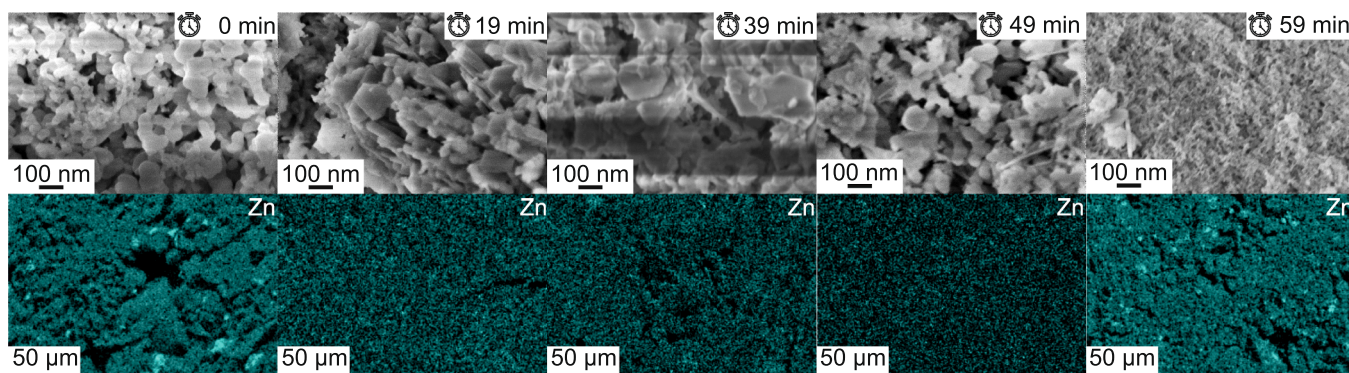

Fig. 3. Morphological changes during suspension ageing (a) and the respective elemental distributions of Zn according to EDXS mapping (b). The other abundant elements (e.g. Cu, Zr, O) were omitted because they did not show differences over time.

IR detection of aging phenomena in CZZ precursor are summarized as follows:

- Tracking of aging development without post-treatment (e.g. washing, drying and preparing KBr pellets)
- Enhanced temporal resolution in contrast to *ex situ* measurements (the latter being restricted by chosen time interval)
- Observation of (potentially relevant) dissolved species

We assigned the most relevant absorption bands to be usable as practicable markers (e.g. CO_3^{2-} asymm. stretching). A precise *in situ* FTIR monitoring during the crucial aging step, without the necessity of a post-treatment is a tremendous advantage as it is also applicable in the up-scaling of a given pre-catalysts' synthesis. This interference-free way of monitoring, together with the compactness of nowadays IR spectrometers allows to directly observe the evolution of amorphous AND crystalline phases. We believe that the general approach, without induced interferences, could contribute to an accelerated development of other precipitation procedures. The herein documented synthesis of a CZZ catalyst precursor for methanol synthesis represents a suitable "case study".

Author contributions

L.W. wrote the manuscript, planned and conducted the synthesis. L. W. and T. Z. performed and analysed the measurements together. Furthermore, T. Z. and S. P. read and revised the manuscript. Additionally, T. Z. and S. P. provided conceptual background for the CZZ catalyst precursor system.

CRediT authorship contribution statement

Lucas Warmuth: Writing – original draft, Supervision, Project administration, Methodology, Investigation, Conceptualization. **Thomas A. Zevaco:** Writing – review & editing, Resources, Methodology, Investigation, Conceptualization. **Stephan Pitter:** Writing – review & editing, Supervision, Methodology, Formal analysis, Conceptualization.

Declaration of competing interest

The authors declare that they have no known competing financial interests or personal relationships that could have appeared to influence the work reported in this paper.

Acknowledgements

Appendix A. Supplementary material

Supplementary data to this article can be found online at https://doi.org/10.1016/j.inoche.2024.113753.

Data availability

The data supporting this article have been included as part of the Supplementary Information.

References

[1] M. Bertau, F. Schmidt, H.-J. Wernicke, H. Offermanns, L. Plass, Methanol: The Basic Chemical and Energy Feedstock of the Future. Asinger's Vision Today, Springer, Berlin, 2014.

[2] R. Schlögl, Chemical batteries with CO2, Angew. Chem. Int. Ed. 61 (2022) e202007397.

[3] K.F. Kalz, R. Kraehnert, M. Dvoyashkin, R. Dittmeyer, R. Gläser, U. Krewer, K. Reuter, J.-D. Grunwaldt, Future challenges in heterogeneous catalysis: understanding catalysts under dynamic reaction conditions, ChemCatChem 9 (2017) 17–29.

[4] S. Navarro-Jaén, M. Virginie, J. Bonin, M. Robert, R. Wojcieszak, A.Y. Khodakov, Highlights and challenges in the selective reduction of carbon dioxide to methanol, Nat. Rev. Chem. 5 (2021) 564–579.

[5] J. Sehested, Industrial and scientific directions of methanol catalyst development, J. Catal. 371 (2019) 368–375.

[6] The Methanol Industry, https://www.methanol.org/the-methanol-industry/, (accessed 11 October 2023).

[7] S. Fujita, A.M. Satriyo, G.C. Shen, N. Takezawa, Mechanism of the formation of precursors for the Cu/ZnO methanol synthesis catalysts by a coprecipitation method, Catal. Lett. 34 (1995) 85–92.

[8] M. Behrens, F. Girgsdies, A. Trunschke, R. Schlögl, Minerals as model compounds for Cu/ZnO catalyst precursors: structural and thermal properties and IR spectra of mineral and synthetic (zincian) malachite, rosasite and aurichalcite and a catalyst precursor mixture, Eur. J. Inorg. Chem. 2009 (2009) 1347–1357.

[9] B. Bems, M. Schur, A. Dassenoy, H. Junkes, D. Herein, R. Schlögl, Relations between synthesis and microstructural properties of copper/zinc hydroxycarbonates, Chemistry 9 (2003) 2039–2052.

[10] J.-L. Li, T. Inui, Characterization of precursors of methanol synthesis catalysts, copper/zinc/aluminum oxides, precipitated at different pHs and temperatures, Appl. Catal. A-Gen. 137 (1996) 105–117.

[11] M. Behrens, R. Schlögl, How to prepare a good Cu/ZnO catalyst or the role of solid state chemistry for the synthesis of nanostructured catalysts, Z. Anorg. Allg. Chem. 639 (2013) 2683–2695.

[12] A. Beck, M.A. Newton, L.G.A. van de Water, J.A. van Bokhoven, The enigma of methanol synthesis by Cu/ZnO/Al2O3-based catalysts, Chem. Rev. (2024), https://doi.org/10.1021/acs.chemrev.3c00148.

[13] S. Wild, S. Polierer, T.A. Zevaco, D. Guse, M. Kind, S. Pitter, K. Herrera Delgado, J. Sauer, Direct DME synthesis on CZZ/H-FER from variable CO2/CO syngas feeds, RSC Adv. 11 (2021) 2556–2564.

[14] E. Lam, K. Larmier, P. Wolf, S. Tada, O.V. Safonova, C. Copéret, Isolated Zr surface sites on silica promote hydrogenation of CO2 to CH3OH in supported Cu catalysts, J. Am. Chem. Soc. 140 (2018) 10530–10535.

[15] S. Tada, A. Katagiri, K. Kiyota, T. Honma, H. Kamei, A. Nariyuki, S. Uchida, S. Satokawa, Cu species incorporated into amorphous ZrO2 with high activity and selectivity in CO2-to-methanol hydrogenation, J. Phys. Chem. C 122 (2018) 5430–5442.

[16] W. Wang, Z. Qu, L. Song, Q. Fu, CO2 hydrogenation to methanol over Cu/CeO2 and Cu/ZrO2 catalysts: tuning methanol selectivity via metal-support interaction, J. Energy Chem. 40 (2020) 22–30.

[17] M. Behrens, Meso- and nano-structuring of industrial Cu/ZnO/(Al2O3) catalysts, J. Catal. 267 (2009) 24–29.

[18] G.C. Shen, S. Fujita, N. Takezawa, Preparation of precursors for the Cu/ZnO methanol synthesis catalysts by coprecipitation methods, J. Catal. 138 (1992) 754–758.

[19] G. Sengupta, D.P. Das, M.L. Kundu, S. Dutta, S.K. Roy, R.N. Sahay, K.K. Mishra, Study of copper-zinc oxide catalysts, characterisation of the coprecipitate and mixed oxide, Appl. Catal. 55 (1989) 165–180.

[20] G.J. Millar, I.H. Holm, P.J.R. Uwins, J. Drennan, Characterization of precursors to methanol synthesis catalysts Cu/ZnO system, Faraday Trans. 94 (1998) 593–600.

[21] D.M. Whittle, A.A. Mirzaei, J.S.J. Hargreaves, R.W. Joyner, C.J. Kiely, S.H. Taylor, G.J. Hutchings, Co-precipitated copper zinc oxide catalysts for ambient temperature carbon monoxide oxidation: effect of precipitate ageing on catalyst activity, PCCP 4 (2002) 5915–5920.

[22] P. Porta, S. de Rossi, G. Ferraris, M.L. Jacono, G. Minelli, G. Moretti, Structural characterization of malachite-like coprecipitated precursors of binary CuO-ZnO catalysts, J. Catal. 109 (1988) 367–377.

[23] S. Zander, B. Seidlhofer, M. Behrens, In situ EDXRD study of the chemistry of aging of co-precipitated mixed Cu,Zn hydroxycarbonates – consequences for the preparation of Cu/ZnO catalysts, Dalton Trans. 41 (2012) 13413.

[24] A. Güldenpfennig, M. Distaso, W. Peukert, In situ investigations on the amorphous to crystalline phase transformation of precursors for methanol synthesis catalysts, Chem. Eng. J. 369 (2019) 996–1004.

[25] P.J. Smith, S.A. Kondrat, P.A. Chater, B.R. Yeo, G.M. Shaw, L. Lu, J.K. Bartley, S.H. Taylor, M.S. Spencer, C.J. Kiely, G.J. Kelly, C.W. Park, G.J. Hutchings, A new class of Cu/ZnO catalysts derived from zincian georgeite precursors prepared by co-precipitation, Chem. Sci. 8 (2017) 2436–2447.

[26] C. Baltes, S. Vukojevic, F. Schuth, Correlations between synthesis, precursor, and catalyst structure and activity of a large set of CuO/ZnO/Al2O3 catalysts for methanol synthesis, J. Catal. 258 (2008) 334–344.

[27] O. Hinrichsen, T. Genger, M. Muhler, Chemisorption of N2O and H2 for the surface determination of copper catalysts, Chem. Eng. Technol. 23 (2000) 956–959.

[28] S. Polierer, D. Guse, S. Wild, K. Herrera Delgado, T.N. Otto, T.A. Zevaco, M. Kind, J. Sauer, F. Studt, S. Pitter, Enhanced direct dimethyl ether synthesis from CO2-rich syngas with Cu/ZnO/ZrO2 catalysts prepared by continuous co-precipitation, Catalysts 10 (2020) 816.

[29] D. Guse, S. Polierer, S. Wild, S. Pitter, M. Kind, Improved preparation of Cu/Zn-based catalysts by well-defined conditions of Co-precipitation and aging, CIT 94 (2022) 314–327.

[30] G. Behrendt, N. Prinz, A. Wolf, L. Baumgarten, A. Gaur, J.-D. Grunwaldt, M. Zobel, M. Behrens, S. Mangelsen, Substitution of copper by magnesium in malachite: insights into the synthesis and structural effects, Inorg. Chem. 61 (2022) 19678–19694.

[31] X. Li, Z.-J. Zhao, L. Zeng, J. Zhao, H. Tian, S. Chen, K. Li, S. Sang, J. Gong, On the role of Ce in CO2 adsorption and activation over lanthanum species, Chem. Sci. 9 (2018) 3426–3437.

[32] Grégory Lefèvre, In situ Fourier-Transform infrared spectroscopy studies of inorganic ions adsorption on metal oxides and hydroxides, https://hal.science/hal-00000940.

[33] F.A. Andersen, L. Brečević, G. Beuter, D.B. Dell'Amico, F. Calderazzo, N.J. Bjerrum, A.E. Underhill, Infrared spectra of amorphous and crystalline calcium carbonate, Acta Chem. Scand. 45 (1991) 1018–1024.

[34] L.V. Volod'ko, L.T. Huoah, The vibrational spectra of aqueous nitrate solutions, J. Appl. Spectrosc. 9 (1968) 1100–1104.

[35] D.J. Goebbert, E. Garand, T. Wende, R. Bergmann, G. Meijer, K.R. Asmis, D.M. Neumark, Infrared spectroscopy of the microhydrated nitrate ions NO(3)(-)(H2O)(1-6), J. Phys. Chem. A 113 (2009) 7584–7592.

[36] M.C. Hales, R.L. Frost, Synthesis and vibrational spectroscopic characterisation of synthetic hydrozincite and smithsonite, Polyhedron 26 (2007) 4955–4962.

[37] D. Stoilova, V. Koleva, V. Vassileva, Infrared study of some synthetic phases of malachite (Cu2(OH)2CO3)–hydrozincite (Zn5(OH)6(CO3)2) series, Spectrochim. Acta, Part A 58 (2002) 2051–2059.

[38] J.C. Lavalley, M. Bensitel, J.P. Gallas, J. Lamotte, G. Busca, V. Lorenzelli, FT-IR study of the d(OH) mode of surface hydroxy groups on metal oxides, J. Mol. Struct. 175 (1988) 453–458.

[39] G. Behrendt, B. Mockenhaupt, N. Prinz, M. Zobel, E.-J. Ras, M. Behrens, CO hydrogenation to methanol over Cu/MgO catalysts and their synthesis from amorphous magnesian georgeite precursors, ChemCatChem 14 (2022), https://doi.org/10.1002/cctc.202200299.

[40] E. Garand, T. Wende, D.J. Goebbert, R. Bergmann, G. Meijer, D.M. Neumark, K.R. Asmis, Infrared spectroscopy of hydrated bicarbonate anion clusters: HCO3(-)(H2O)(1-10), J. Am. Chem. Soc. 132 (2010) 849–856.

[41] B.H. Solis, Y. Cui, X. Weng, J. Seifert, S. Schauermann, J. Sauer, S. Shaikhutdinov, H.-J. Freund, Initial stages of CO2 adsorption on CaO: a combined experimental and computational study, PCCP 19 (2017) 4231–4242.

[42] J. Schumann, A. Tarasov, N. Thomas, R. Schlögl, M. Behrens, Cu,Zn-based catalysts for methanol synthesis: on the effect of calcination conditions and the part of residual carbonates, Appl. Catal. A-Gen. 516 (2016) 117–126.

[43] W. Vetter, I. Latini, M. Schreiner, Azurite in medieval illuminated manuscripts: a reflection-FTIR study concerning the characterization of binding media, Heritage Sci. 7 (2019) 21.

[44] G.C. Jones, B. Jackson, Infrared Transmission Spectra of Carbonate Minerals, first edition, Springer, 1993.

[45] M. Behrens, Meso- and nano-structuring of industrial Cu/ZnO/(Al2O3) catalysts, J. Catal. 267 (1) (2009) 24–29.